Bonding of Xenon Hydrides

Nancy Pérez-Peralta,[†] Rosalba Juárez,[†] Erick Cerpa,[†] F. Matthias Bickelhaupt,*[,‡] and Gabriel Merino*[,†]

Departamento de Química, Universidad de Guanajuato, Col. Noria Alta s/n, CP 36050, Guanajuato, Gto., Mexico, and Department of Theoretical Chemistry and Amsterdam Center for Multiscale Modeling, Scheikundig Laboratorium der Vrije Universiteit, De Boelelaan 1083, NL-1081 HV Amsterdam, The Netherlands

Received: April 9, 2009; Revised Manuscript Received: July 4, 2009

We have computed the structure and stability of the xenon hydrides HXeY (with Y = F, Cl, Br, I, CCH, CN, NC) using relativistic density functional theory (DFT) at ZORA-BP86/TZ2P level. All model systems HXeY studied here are bound equilibrium structures, but they are also significantly destabilized with respect to Xe and HY. We have analyzed the bonding in HXeY in order to arrive at a simple picture that explains the main trends in stability.

Introduction

In 1933 Pauling proposed that it should be possible to obtain noble-gas compounds, at least from the heavier gases krypton and xenon.[1] The proof for Pauling's suggestion came in 1962 when Bartlett synthesized $XePtF_6$.[2] Since Bartlett's discovery, several complexes containing a noble-gas (Ng) atom have been detected experimentally or proposed on paper.[3−9]

One recent source of interest in this field is the noble-gas hydride chemistry, in particular the HNgY type complexes (H = hydrogen atom, Ng = noble-gas atom, and Y = electronegative fragment). They have been studied both experimentally and computationally since their discovery in 1995.[10] Right now this intriguing family has 23 members, and all of them are prepared in noble-gas matrices.[4] The Y moiety is not restricted to inorganic ligands. In 2002, Lundell et al. proposed that Xe can be inserted also into hydrocarbon H−C bonds.[11] They found that some molecules such as HXeCCH, $HXeC_6H_5$, and $HXeOC_6H_5$ could exist *in silico*. The first experimental evidence of HXeCCH was published independently by Khriachtchev et al.[12] and Feldman et al.[13] More recently, HKrCCH,[14] $HXeC_4H$,[15] and $HKrC_4H$[15] were also obtained experimentally by photolysis of a hydrocarbon in a noble-gas matrix.

But the underlying nature of the chemical bonding in these remarkable complexes is not yet fully understood. In this paper, we present for the first time a systematic study of the nature of the Ng−H and Ng−Y bonding in the title systems using density functional theory (DFT) at BP86/TZ2P, as implemented in the Amsterdam Density Functional (ADF) program.[16] In particular, we analyze the Ng−H and Ng−Y bonding mechanism in the framework of the quantitative molecular orbital (MO) model contained in the Kohn−Sham approach to DFT, in combination with an energy decomposition analysis (EDA).[17−21] This enables us to understand how the bonding comes about and to quantify the relative importance of different bonding terms, such as electrostatic attraction and orbital interactions.

Computational Details

All geometries have been optimized at the nonlocal DFT level using the exchange functional of Becke[22] with the correlation functional of Perdew[23] (BP86) in ADF2008.[16] Molecular orbitals (MOs) were expanded in a basis set consisting of a set of uncontracted Slater-type orbitals (STOs).[24] The basis sets have triple-ζ quality augmented by two sets of polarization functions, that is, p and d functions for the hydrogen atoms and d and f functions for the other atoms. This level is denoted as BP86/TZ2P. An auxiliary set of s, p, d, f, and g STOs was used to fit the molecular densities and to represent the Coulomb and exchange potentials accurately in each SCF cycle. Atomic charges are computed using Voronoi deformation density (VDD) method[25] as well as the Hirshfeld method.[26] Scalar relativistic effects have been considered using the zero-order regular approximation (ZORA).[27−31]

Bonding Analysis

To obtain more insight into the nature of the bonding mechanism between the noble-gas atom (Xe) and the H- - -Y fragment in our H−Xe−Y model systems, an energy decomposition analysis (EDA) has been carried out.[17−21] Here, the total bonding energy ΔE associated with forming the overall molecular species of interest, HXeY, from the two fragments, Xe + HY, is made up of three major components (eq 1):

$$\mathrm{Xe} + \mathrm{HY} \rightarrow \mathrm{HXeY}: \qquad \Delta E = \Delta E_{\mathrm{set}} + \Delta E_{\mathrm{geom}} + \Delta E_{\mathrm{int}} \tag{1}$$

In this formula, ΔE_{set} is the vertical single electron transfer energy, i.e., the energy required to transfer one electron from Xe to the fragment HY which, however, remains in the equilibrium structure of the neutral species (eq 2):

$$\mathrm{Xe} + \mathrm{HY} \rightarrow \mathrm{Xe}^{+\bullet} + [\mathrm{HY}^{-\bullet}]_{\mathrm{HY}}: \qquad \Delta E_{\mathrm{set}} \tag{2}$$

Furthermore, ΔE_{geom}, is the energy change associated with elongating the H−Y bond distance to the value it adopts in the overall molecule HXeY (eq 3):

$$[\mathrm{HY}^{-\bullet}]_{\mathrm{HY}} \rightarrow [\mathrm{HY}^{-\bullet}]_{\mathrm{HXeY}}: \qquad \Delta E_{\mathrm{geom}} \tag{3}$$

[†] Universidad de Guanajuato.
[‡] Scheikundig Laboratorium der Vrije Universiteit.

10.1021/jp903266a CCC: $40.75
Published on Web 08/06/2009

And finally, ΔE_{int} is the energy change associated with bringing the fragments $Xe^{+\bullet}$ and $[HY^{-\bullet}]_{HXeY}$ together to form HXeY (eq 4):

$$Xe^{+\bullet} + [HY^{-\bullet}]_{HXeY} \rightarrow HXeY: \qquad \Delta E_{int} \tag{4}$$

The electron-transfer step is introduced for two reasons: (i) our analyses of the electronic structure show that there is a significant transfer of negative charge in HXeY from Xe to HY (*vide infra*); (ii) this is so because the *neutral* $[HY]_{HXeY}$ fragment in the geometry of the overall molecule has a very low-energy σ^* LUMO because of the long H- - -Y bond: this results in a near (or virtually perfect) $\sigma-\sigma^*$ degeneracy and, consequently, an oscillating, nonconverging SCF process. This process is resolved as the σ^* is populated with one electron (and thus pushed up in energy) as it occurs also in the overall HXeY complex. Finally, we will complement the above decomposition with alternative fragmentations of the model systems into $H-Xe^+$ and Y^- units (HXe···Y bonding) and into $H^\bullet + XeY^\bullet$ units (H···XeY bonding).

The interaction energy ΔE_{int} is further analyzed in the framework of the Kohn−Sham molecular orbital (MO) model using a quantitative decomposition of the bond into electrostatic interaction, Pauli repulsion (or exchange repulsion or overlap repulsion), and (attractive) orbital interactions (eq 5):

$$\Delta E_{int} = \Delta V_{elstat} + \Delta E_{Pauli} + \Delta E_{oi} \tag{5}$$

The term ΔV_{elstat} corresponds to the classical electrostatic interaction between the unperturbed charge distributions $\rho_{Xe+\bullet}(\mathbf{r}) + \rho_{[HY-\bullet]HXeY}(\mathbf{r})$ of the radical fragments $Xe^{+\bullet}$ and $[HY^{-\bullet}]_{HXeY}$ that adopt their positions in the overall molecule HXeY and is, as this term usually is, attractive. The Pauli repulsion term, ΔE_{Pauli}, comprises the destabilizing interactions between occupied orbitals and is responsible for the steric repulsion. This repulsion is caused by the fact that two electrons with the same spin cannot occupy the same region in space. It arises as the energy change associated with the transition from the superposition of the unperturbed electron densities $\rho_{Xe+\bullet}(\mathbf{r}) + \rho_{[HY-\bullet]HXeY}(\mathbf{r})$ of the geometrically deformed but isolated radical fragments A and B to the wave function $\Psi^0 = N\hat{A}[\Psi_{Xe+\bullet}\Psi_{[HY-\bullet]HXeY}]$, that properly obeys the Pauli principle through explicit antisymmetrization ($\hat{A}$ operator) and renormalization (N constant) of the product of fragment wave functions (see ref 17 for an exhaustive discussion). The orbital interaction ΔE_{oi} in any MO model, and therefore also in Kohn−Sham theory, accounts for electron-pair bonding, charge transfer (i.e., donor−acceptor interactions between occupied orbitals on one moiety with unoccupied orbitals of the other, including the HOMO−LUMO interactions; $SOMO_{Xe+\bullet}-SOMOH_{Y-\bullet}$ interactions in our particular partitioning scheme) and polarization (empty-occupied orbital mixing on one fragment due to the presence of another fragment). In the bond-energy decomposition, open-shell fragments are treated with the spin-unrestricted formalism but, for technical (not fundamental) reasons, spin-polarization is not included. This error causes an electron-pair bond to become in the order of a few kcal·mol^{-1} too strong. To facilitate a straightforward comparison, the results of the energy decomposition were scaled to match exactly the regular bond energies. Since the Kohn−Sham MO method of density-functional theory (DFT) in principle yields exact energies and, in practice, with the available density functionals for exchange and correlation, rather accurate energies, we have the special situation that a seemingly one-particle model (an MO method) in principle completely accounts for the bonding energy.[17]

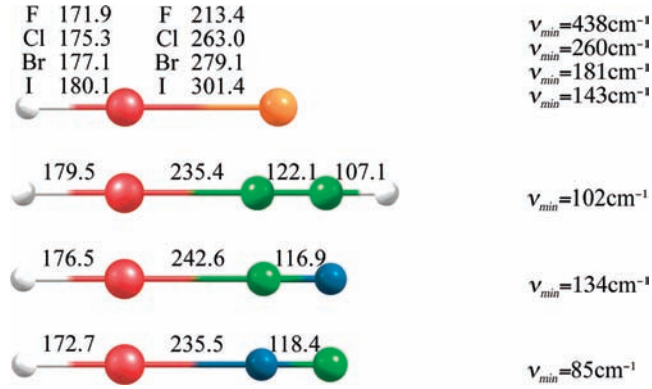

Figure 1. Optimized structures (in pm) at the BP86/TZ2P level for HXeY with Y = F, Cl, Br, I, C_2H, CN and NC, respectively. ν_{min} is the smallest vibrational frequency of every molecule.

The orbital interaction energy can be decomposed into the contributions from each irreducible representation Γ of the interacting system (eq 6) using the extended transition state (ETS) scheme developed by Ziegler and Rauk[18−20] (note that our approach differs in this respect from the Morokuma scheme,[21,32] which instead attempts a decomposition of the orbital interactions into polarization and charge transfer):

$$\Delta E_{oi} = \sum_{\Gamma} \Delta E_{\Gamma} = \Delta E_{\sigma} + \Delta E_{\pi} \tag{6}$$

Structure

Figure 1 displays the geometrical parameters calculated at the BP86/TZ2P level for the HXeY systems. In all cases, the local coordination environment at Xe is linear. The HXeY structures have been described extensively in several places in the literature. For details we refer the reader to ref 4. Frequency calculations show that each structure depicted in Figure 1 is a local minimum on its corresponding potential energy surface. In the case of the halogen complexes, the smallest vibrational frequency (ν_{min}) corresponds to an asymmetric stretching vibrational mode, while ν_{min} for HXeCCH, HXeCN, and HXeNC is related to a bending mode.

Traditionally density functional theory (DFT) methods, including BP86, are not necessarily reliable for systems dominated by *dispersion*. However, Table 1 shows that the calculated Xe−Y and Xe−H distances at the BP86/TZ2P level are in agreement with the bond lengths obtained at different high levels of theory using in early contributions (see Table 1). The main reason for the correct DFT description of the HXeY complexes is the presence of strong bonding, which is not a simple longer-range nonbonded attractive interaction. Recently, Lignell et al.[33] and Panek et al.[34] discussed the status and reliability of theoretical predictions of noble-gas hydride. They found that the DFT methods offer an attractive alternative to study large HNgY species. Thus, we can assume, based on previous discussion, that BP86/TZ2P is a reasonable level to study the bonding situation of xenon hydrides.

Dissociation Barriers

All the species studied here correspond to local minima on the potential energy surface. Even though these structures are local minima, its experimental detection strongly depends on

TABLE 1: Comparison of Bond Distances (in pm) in HXeY Complexes Optimized at BP86/TZ2P with Previous Results

	method	R_{Xe-H}	R_{Xe-Y}	ref
HXeF	BP86/TZ2P	171.9	213.8	
	UMP2/43333/4333/43(Xe)/6-31G**(F)/6-311G**(H)	166.9	213.9	10
HXeCl	BP86/TZ2P	175.6	263.4	
	UMP2/LANL1DZ	180.9	278.4	10
	UMP2/ECP(Xe)/WBP(Cl)/6-311G**(H)	181.0	282.3	10
	UMP2/43333/4333/43(Xe)/533/5111(Cl)/6-311G**(H)	167.4	285.2	10
HXeBr	BP86/TZ2P	177.4	279.4	
	UMP2/LANL1DZ	186.9	297.8	10
	UMP2/ECP(Xe,Br)/6-311G**(H)	184.9	301.3	10
	UMP2/43333/4333/43(Xe)/4333/433/4(Br)/6-311G**(H)	178.0	297.8	10
HXeI	BP86/TZ2P	180.3	301.9	
	UMP2/LANL1DZ	204.3	323.9	10
	UMP2/ECP(Xe,I)/+$VP^S(2p)^S$	191.6	325.9	10
	UMP2/43333/4333/43(Xe,I)/6-311G**(H)	181.4	322.2	10
HXeCCH	BP86/TZ2P	179.6	236.1	
	MP2/LJ18/6-311++G(2d,2p)	175.0	232.2	11
HXeCN	BP86/TZ2P	176.7	243.3	
	MP2/LJ18/6-311++G(2d,2p)	170.7	239.2	35
	MP2/R18/6-311++G(2d,2p)	171.8	237.1	35
HXeNC	BP86/TZ2P	173.0	236.0	
	MP2/LJ18/6-311++G(2d,2p)	165.9	234.2	35
	MP2/R18/6-311++G(2d,2p)	167.0	230.7	35

the magnitudes of the energy barriers that prevent distortion or fragmentation (HNgY into Ng + HY or H + Ng + Y). To be experimentally detected in a given technique, the time needed to go from one minimum to another must be larger than the detection time. So, energy differences between the species and corresponding transition states were computed for the systems studied. However, the BP86 functional that we use here tends to underestimate the transition barrier heights. In this sense, our BP86/TZ2P results are only a crude estimation of these barriers. Recently, multireference CASPT2 calculations for the decomposition of HXeCCH into Xe + HCCH yielded results different from those obtained by MP2.[36]

Here only the reaction paths related to the bendinglike motions of the H atom toward Xe of HXeY were computed at the BP86/TZ2P level (Figure 2). Clearly, this two-body decomposition channel is not so probable at practical temperatures since the barriers (over 29 kcal·mol^{-1}) are very high. So, our results indicate that all the title complexes are kinetically stable with respect to the Ng + HY exoergic decomposition channel.

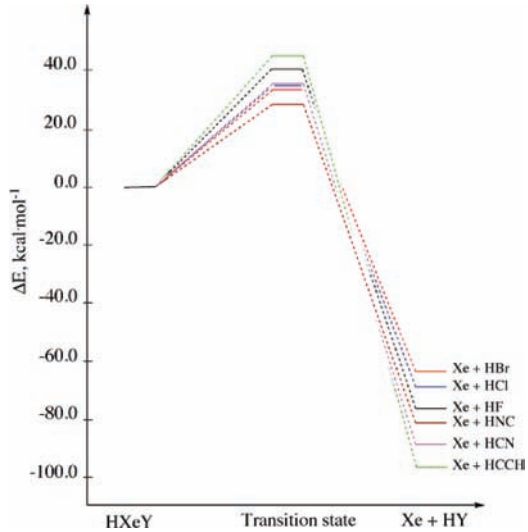

Figure 2. Paths for the bending-like motions of the H atom toward the Xe of HXeY calculated at the BP86/TZ2P level including the ZPE correction. We were not able detect the corresponding transition state for the HXeI complex.

SCHEME 1

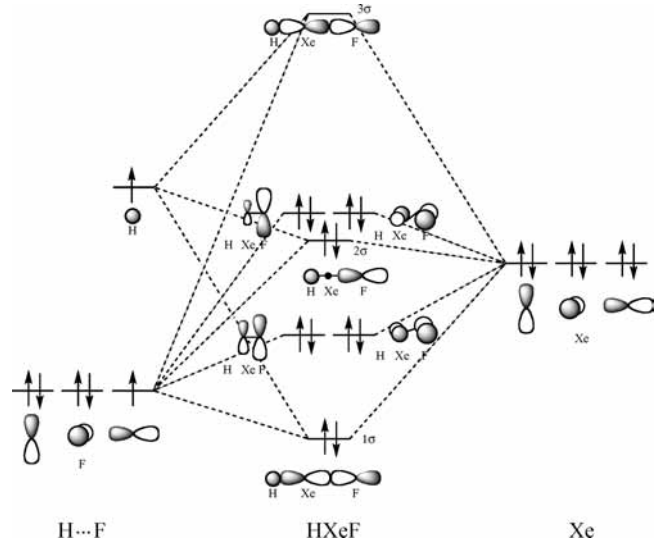

Molecular Orbital Analysis

At the risk to repeat what is obvious, let us start with the simplest system, HXeF. Similar to XeF_2, the bonding in this molecule can be understood using the classical Pimentel−Rundle three-center model.[37,38] In this case, the linear H−Xe−F unit is described by three molecular orbitals (MOs) derived from the collinear p-orbitals in the Xe and F atoms and the s orbital in the H atom (see Scheme 1). The bonding results from the combination of a filled p-orbital in the central atom with two half-filled orbitals provided by the p-orbital in the fluorine atom and by the s-orbital in H, resulting in a filled bonding orbital (1σ, see Scheme 1), a filled nonbonding orbital (2σ), and one antibonding orbital (3σ). Indeed, our calculations show that the hypervalent coordination sphere of xenon is not brought about by the participation of xenon d-orbitals which contribute only some 7%, supporting the presence of a 3-center-four-electron bond. However, using this diagram it is not so simple to quantify the orbital and the electrostatic contributions.

Last and George[39] proposed to conceive the H−Xe−Y species as being built up in two steps: the first step is transfer of one electron from the closed-shell Xe atom to the electronegative

SCHEME 2

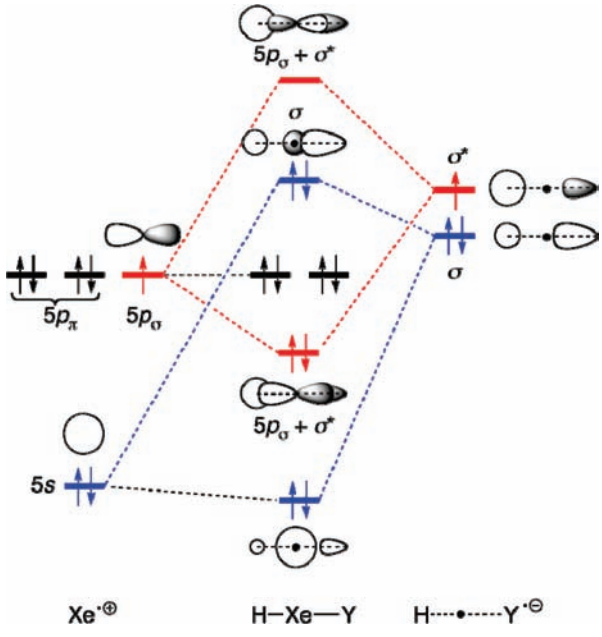

group Y to yield the neutral Xe^+-Y^- subunit, which involves a large expense of energy that is only partially compensated by the electron affinity of Y and Coulombic attraction between Y^- and Xe^+. The second step involves the interaction of an unpaired electron in a p-type orbital of the Y^-Xe^+ fragment with the unpaired s electron of the H atom. The result is the formation of a strong σ bond. This picture is eventually equivalent to the simple Pimentel−Rundle model.

Bonding Mechanism

Scheme 2 is different from the previous one. Here, the electron-transfer step is introduced. Our analyses of the electronic structure show that there is a significant transfer of negative charge in HXeY from Xe to HY (*vide infra*). This is because the neutral $[HY]_{HXeY}$ fragment in the geometry of the overall molecule has a very low energy σ^* SOMO because of the long H- - -Y bond, resulting in a near (or virtually perfect) $\sigma-\sigma^*$ degeneracy. This new scheme yields a clear and simple picture of the xenon−ligand bonding between in HXeY: the bonding results from a polar electron-pair bond between the $Xe^{+\bullet}$ $5p_\sigma$ SOMO and $[H- - -Y^{-\bullet}]$ σ^* SOMO (red levels in Scheme 2). In the course of this interaction, 0.16 |e$^-$| (HXeF) to 0.36 |e$^-$| (HXeI) flow from the radical anion to the noble-gas radical cation (see Table 2). This is also reflected by both Hirshfeld and VDD atomic charges for xenon of ca. +0.4 |e$^-$|.

Thus, in terms of the Gross population of the σ^* fragment orbital, 60−80% of the excess electron remains on the electronegative $[H- - -Y^{-\bullet}]$ moiety. Furthermore, the closed-shell $[H- - -Y^{-\bullet}]$ σ orbital is relatively little affected owing to the very poor overlap (cancellation of overlap, see blue level in Scheme 2). This can also be conceived as a H−Xe−Y 3-center-4-electron orbital-interaction pattern which corresponds to the classical Pimentel−Rundle model.[37,38] Note also that the large population of the σ^* on $[H- - -Y^{-\bullet}]$ nicely matches with our two-step approach to analyzing the bonding in HXeY by first transferring an electron from Xe to HY which is also reminiscent of the earlier proposal by Last and George. However, we recall that charge separation between Xe and HY prior to formation of the overall HXeY complex, i.e., reaction 2, is unfavorable in terms of energies and rather serves as a concept of an understanding how the final wave function arises from the initial reactants (*vide infra*).

Bond Energy Decomposition

Next, we consider the trends in bonding along the different HXeY model systems more quantitatively. In all cases, the HXeY systems are substantially, i.e., by 60 − 100 kcal·mol^{-1}, destabilized with respect to Xe + HY (see Table 2). The main reason is the loss of H−Y bonding which is not compensated by the relatively poor interaction with the central noble-gas atom. Thus, the charge separation associated with single-electron transfer from Xe to HY (reaction 2) is strongly endothermic with values ranging from ΔE_{set} = 297 to 334 kcal·mol^{-1}. This transfer of one full electron is of course an exaggeration with respect to the situation in the final HXeY complex, in which charge is donated back to $Xe^{+\bullet}$ (*vide supra*). Yet, as mentioned before, much of the excess negative charge does remains in the σ^* orbital of the $[H- - -Y^{-\bullet}]_{HXeY}$ fragment in HXeY.

The combined action of both electrostatic attraction ΔV_{elstat} and bonding orbital interactions ΔE_{oi} in HXeY is insufficient to compensate for the large destabilization by ΔE_{set}. The reason is the Pauli repulsion of $H- - -Y^{-\bullet}$ with the closed shells of $Xe^{+\bullet}$, mainly between $Xe^{+\bullet}$ 5s and $H- - -Y^{-\bullet}$ σ (see blue levels in Scheme 2 and ΔE_{Pauli} in Table 2). This term, ΔE_{Pauli}, generates a repulsive wall that prevents the stabilizing interactions from growing stronger at shorter bond distances. Thus, the electrostatic attraction weakens as the H−Xe and Xe−Y bond distances become longer, e.g. along Y = F, Cl, Br and I (see Table 2).

The orbital interactions, which mainly stem from the σ-electron system, also decrease along Y = F, Cl, Br and I. This is not so much due to a decreasing overlap which remains ∼0.47 along this series. Rather, it originates from a decreasing electronegativity difference between $Xe^{+\bullet}$ and $[H- - -Y^{-\bullet}]_{HXeY}$. Thus, as the energy of the $[H- - -Y^{-\bullet}]_{HXeY}$ σ^* drops, the unpaired electron stemming from this orbital receives less stabilization as it "drops" into the electron-pair bonding $5p_\sigma + \sigma^*$ MO in HXeY.[40] Note that the situations for HXeCCH, HXeCN and HXeNC are intermediate in terms of both Xe−Y bond distances and electrostatic and orbital interactions.

It is the trends in ΔE_{set} and ΔE_{geom}, not the net interaction, ΔE_{int}, that determine the overall trend in stability. Thus, HXeY becomes more stable with respect to Xe + HY (i.e., ΔE becomes less endothermic) along HY = HCCH, HCN, HNC, F, Cl, Br, and I. This matches exactly the trend in ΔE_{set}, which decreases from 335 to 297 kcal·mol^{-1}. On the other hand, the HY σ^* energies have no relation with the other energetic terms. The geometrical deformation energy behaves somewhat less regularly but it is also much smaller than the ΔE_{set}. But, along the series of hydrogen halides, i.e., HF, HCl, HBr, and HI, ΔE_{geom} becomes systematically more stabilizing, going from 24.7 to −5.2 to −8.6 to −9.4 kcal/mol. These trends dominate the counteracting trend in ΔE_{int} and cause the overall stabilization of HXeY along this series.

Heterolytic Picture of HXe···Y Bonding

Next, we will look from a different perspective at the bonding in our model systems, namely, by focusing on the individual H···XeY and HXe···Y bonds. We first used the $H-Xe^+$ and Y^- units as interacting fragments which corresponds to a heterolytic picture of the HXe···Y bonding (see Table 3). Lein et al. have done a similar energy partitioning analysis for HArF.[41] In our case, clearly the strength of the interactions decreases in the order F > Cl > Br > I. The absolute value of the electrostatic and the Pauli repulsion terms for the fluorine

TABLE 2: Analysis of the Element−Xenon Bonding Mechanism between $Xe^{+\bullet}$ and $[H\text{-}\text{-}\text{-}Y]^{-\bullet}$ in H−Xe−Y[a]

	HXeF	HXeCl	HXeBr	HXeI	HXeCCH	HXeCN	HXeNC
			Geometry (in pm)				
H−Xe	171.9	175.3	177.1	180.1	179.5	176.5	172.7
Xe−Y	213.4	263.0	279.1	301.4	235.4	242.6	235.5
			Bond Energy Decomposition (in kcal mol^{-1})[b]				
ΔE_{oi}	–179.0	–162.4	–160.7	–158.1	–167.1	–162.0	–166.7
ΔE_{σ}	–162.1	–150.7	–149.7	–148.2	–153.6	–151.6	–150.8
ΔE_{π}	–16.9	–11.7	–11.0	–9.9	–13.5	–10.4	–15.9
ΔE_{Pauli}	212.4	174.6	165.8	153.7	197.2	178.1	189.8
ΔV_{elstat}	–296.6	–251.1	–239.4	–224.1	–282.8	–254.7	–255.9
ΔE_{int}	–263.2	–239.1	–234.3	–228.5	–252.7	–238.6	–232.8
ΔE_{geom}	24.7	–5.2	–8.6	–9.4	17.5	1.0	–4.6
ΔE_{set}	316.8	313.1	306.0	297.9	334.7	328.8	320.7
$\Delta E = -D_e$	78.3	68.8	63.1	60.0	99.5	91.2	83.3
			$\langle Xe^{\bullet+}$: $5p_{\sigma}$ | $[H\cdots Y^{\bullet-}]$: $\sigma^*\rangle$ Fragment Orbital Overlap				
$\langle SOMO_{Xe}\bullet+$?>|$SOMO_{H\text{-}\text{-}\text{-}Y}\bullet-\rangle$	0.47	0.47	0.46	0.47	0.52	0.49	0.44
			Fragment Orbital Energy (in eV)				
$Xe^{\bullet+}$: $5p_{\sigma}$	–17.59						
$[H\cdots Y^{\bullet-}]$: σ^*	–0.64	–1.12	–1.21	–1.27	–0.95	–1.19	–1.24
$[HY^{\bullet-}]$: σ^*	4.26	4.02	3.66	3.21	4.07	4.44	4.29
			Fragment Orbital Population (in Electrons)				
$Xe^{\bullet+}$: $5p_{\sigma}$	1.16	1.29	1.31	1.36	1.29	1.30	1.26
$[H\cdots Y^{\bullet-}]$: σ^*	0.81	0.68	0.64	0.59	0.69	0.68	0.76
			VDD Atomic and Fragment Charge (in au)				
q^{VDD}(H)	0.027	0.032	0.025	0.012	–0.045	0.014	0.050
q^{VDD}(Xe)	0.371	0.404	0.400	0.375	0.405	0.418	0.423
q^{VDD}(Y)	–0.399	–0.435	–0.425	–0.387	–0.360	–0.431	–0.473
			Hirshfeld Atomic and Fragment Charge (in au)				
$q^{Hirshfeld}$(H)	–0.005	–0.004	–0.009	–0.020	–0.066	–0.023	0.009
$q^{Hirshfeld}$(Xe)	0.420	0.414	0.405	0.384	0.413	0.455	0.484
$q^{Hirshfeld}$(Y)	–0.415	–0.411	–0.396	–0.364	–0.347	–0.432	–0.492

[a] Computed at BP86/TZ2P. [b] $\Delta E = \Delta E_{prep} + \Delta E_{int} = \Delta E_{set} + \Delta E_{geom} + \Delta V_{elstat} + \Delta E_{Pauli} + \Delta E_{oi}$. See also the computational details section.

TABLE 3: EDA Results for HXeY (Y = F, Cl, Br, I, CCH, CN, and NC) at the BP86/TZ2P Level Using the HXe^+ and Y^- as Fragments[a]

	HXeF	HXeCl	HXeBr	HXeI	HXeCCH	HXeCN	HXeNC
ΔE_{oi}	−83.3	−70.8	−71.6	−72.6	−97.4	−76.8	−66.3
	(28%)	(31%)	(32%)	(34%)	(31%)	(31%)	(29%)
ΔE_{σ}	−68.9	−60.6	−61.8	−63.7	−84.2	−68.4	−54.8
	(83%)	(86%)	(86%)	(88%)	(87%)	(89%)	(83%)
ΔE_{π}	−14.5	−10.2	−9.8	−8.8	−13.1	−8.5	−11.5
	(17%)	(14%)	(14%)	(12%)	(13%)	(11%)	(17%)
ΔE_{Pauli}	113.0	81.2	78.2	71.3	152.8	100.7	88.4
ΔV_{elstat}	−209.9	−159.8	−151.0	−138.3	−220.3	−174.1	−163.7
	(72%)	(69%)	(68%)	(66%)	(69%)	(69%)	(71%)
ΔE_{int}	−180.2	−149.4	−144.4	−139.5	−164.8	−150.1	−141.6
ΔE_{geom}	1.6	2.8	3.6	5.0	5.4	3.6	1.9
$\Delta E = -D_e$	−178.6	−146.6	−140.9	−134.6	−159.4	−146.6	−139.7

[a] Energy values are given in kcal·mol^{-1}.

complex are also much higher than for the heavier homologues. Note that the ΔE_{oi} term in the linear HXeY structures increase from 28% in F to 34% in I. The much larger stabilization by the electrostatic attraction ΔV_{elstat} is the result of the energetically highly unfavorable charge separation between the two fragments HXe^+ and Y^-. Apparently, the largest part of ΔE_{oi} comes from σ orbitals, however, the π contribution is not negligible and decrease gradually from F (17%) to I (12%). These trends are a consequence of the decrease of electron transfer from the Ng atom to the halogen atom when the latter gets heavier and less electronegative.

When Y is an acetylenic group, the EDA calculations predict that the interaction energy between both fragments is intermediate between HXeF and HXeCl ($\Delta E_{int} = -164.4$ kcal·mol^{-1}, see Table 3). Note that the magnitude of both the electrostatic and the orbital contributions for HXeCCH are the largest of all of the complexes selected in this study. However, the Pauli repulsion ΔE_{Pauli} is substantial and reduces the absolute value of the interaction energy. Here again, the largest component of the attraction is the electrostatic term (69%). The orbital attraction $\Delta E_{oi} = -96.1$ kcal·mol^{-1} is weaker than the electrostatic one, and its main contribution comes from the σ orbitals (87%). From this point of view, the $HXe^+\cdots{}^-CCH$ interaction is 69% electrostatic.

It is also interesting to extend this discussion to the stability of HXeCN and HXeNC. Note that HXeCN has a higher interaction energy ($\Delta E_{int} = -150.2$ kcal·mol^{-1}) than HXeNC ($\Delta E_{int} = -141.6$ kcal·mol^{-1}). Similar to all xenon hydrides, the EDA values indicate that the attractive interaction between the HXe^+ and Y^- come from the electrostatic term. The partition of the orbital term into contributions by the orbitals shows that the σ bonding is larger for HXeCN.

Homolytic Picture of H···XeY Bonding

Now, let us analyze the H···XeY bonding. From Scheme 3, it is easy to justify that in this case the best partition is using H and XeY as fragments. In this case, the largest contribution to the ΔE_{int} comes from the orbital term, which contributes with ~58% to the binding energy. The electrostatic contribution is thus smaller but not negligible (~42%). In fact, there is a small electron transfer from Xe to H (Scheme 3), justifying the considerable atomic charge in the hydrogen atom (see Table 4). The calculated data suggest that the σ orbitals are the most important orbitals for the ΔE_{oi} term. The strength of the interactions decreases in the order F > CCH ~ NC > CN > Cl > Br > I. Interestingly, there is a linear correlation between ΔE_{oi} and the Xe−H bond lengths (Figure 3).

SCHEME 3

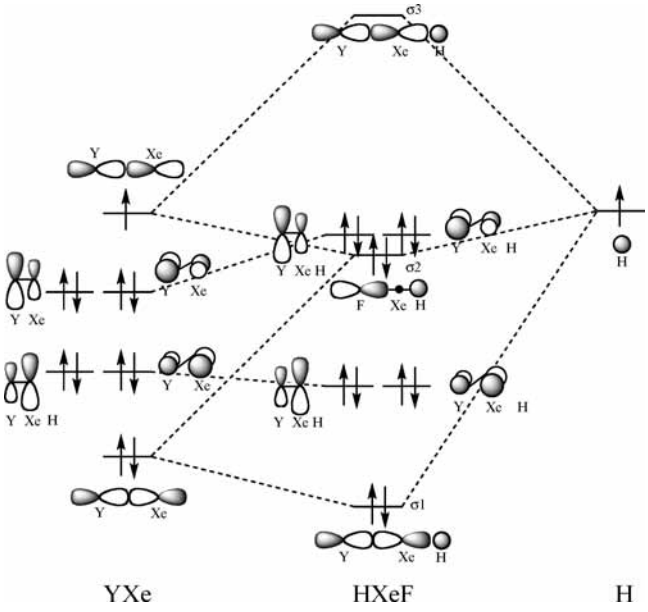

TABLE 4: EDA Results for HXeY (Y = F, Cl, Br, I, CCH, CN, and NC) at the BP86/TZ2P Level Using the H˙ and ˙XeY as Fragments[a]

	HXeF	HXeCl	HXeBr	HXeI	HXeCCH	HXeCN	HXeNC
ΔE_{oi}	−89.1	−79.7	−74.9	−67.0	−73.8	−79.4	−88.5
	(59%)	(59%)	(58%)	(57%)	(59%)	(59%)	(59%)
ΔE_{σ}	−86.5	−77.5	−72.8	−65.3	−72.4	−77.6	−85.9
	(97%)	(97%)	(97%)	(98%)	(98%)	(98%)	(97%)
ΔE_{π}	−2.6	−2.2	−2.0	−1.7	−1.4	−1.8	−2.6
	(3%)	(3%)	(3%)	(2%)	(2%)	(2%)	(3%)
ΔE_{Pauli}	100.1	99.2	97.3	92.5	84.8	94.8	108.5
ΔV_{elstat}	−61.2	−56.4	−54.2	−50.2	−52.2	−55.4	−61.9
	(41%)	(41%)	(42%)	(43%)	(41%)	(41%)	(41%)
ΔE_{int}	−50.1	−36.8	−31.7	−24.8	−41.2	−40.0	−41.9
ΔE_{geom}	2.8	3.5	3.6	4.4	5.1	4.7	9.7
$\Delta E = -D_e$	−47.4	−33.3	−28.1	−20.3	−36.1	−35.3	−32.2

[a] Energy values are given in kcal·mol^{-1}.

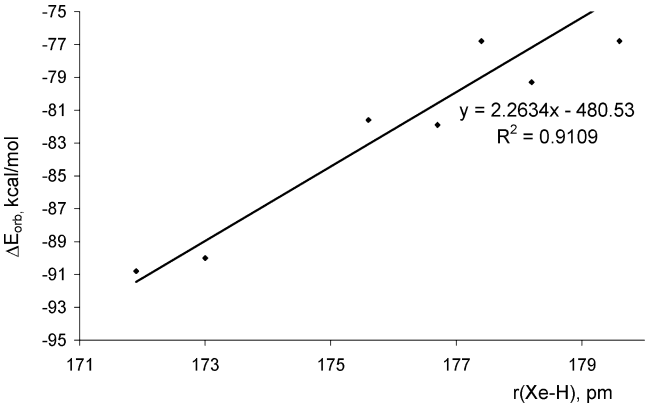

Figure 3. Correlation of orbital contribution to the interaction energy (ΔE_{orb}) with the Xe−H bond lengths.

Conclusions

Xenon hydrides HXeY (with Y = F, Cl, Br, I, CCH, CN, NC) are all bound equilibrium structures as follows from our relativistic density functional theory (DFT) at the ZORA-BP86/TZ2P level. Our results show that the bonding between Xe and H- - -Y results from a polar σ electron-pair bond. However, the computations also show that all the noble-gas compounds are significantly (60−100 kcal·mol^{-1}) destabilized with respect to Xe and HY. The main reason is the interruption of the HY bond which is by far not compensated by H−Xe and Xe−Y bonding.

Acknowledgment. This work was supported by Conacyt (Grant 57892). E.C. and N.P.-P. thank Conacyt for the PhD fellowships. F.M.B. thanks The Netherlands Organization for Scientific Research (NWO-CW and NWO-NCF) for financial support. We dedicate this paper to Prof. Jose Luis Gazquez on the occasion of his 60th birthday and in appreciation of his seminal contributions to the conceptual DFT.

References and Notes

(1) Pauling, L. *J. Am. Chem. Soc.* **1933**, *55*, 1895.
(2) Bartlett, N. *Proc. Chem. Soc.* **1962**, 218.
(3) Frohn, H. J.; Bardin, V. V. *Organometallics* **2001**, *20*, 4750.
(4) Khriachtchev, L.; Rasanen, M.; Gerber, R. B. *Acc. Chem. Res.* **2009**, *42*, 183.
(5) Grochala, W. *Chem. Soc. Rev.* **2007**, *36*, 1632.
(6) Frenking, G.; Koch, W.; Gauss, J.; Cremer, D. *J. Am. Chem. Soc.* **1988**, *110*, 8007.
(7) Laszlo, P.; Schrobilgen, G. J. *Angew. Chem., Int. Ed. Engl.* **1988**, *27*, 479.
(8) Jimenez-Halla, O. C.; Fernandez, I.; Frenking, G. *Angew. Chem., Int. Ed.* **2009**, *48*, 366.
(9) Yen, S. Y.; Mou, C. H.; Hu, W. P. *Chem. Phys. Lett.* **2004**, *383*, 606.
(10) Pettersson, M.; Lundell, J.; Rasanen, M. *J. Chem. Phys.* **1995**, *102*, 6423.
(11) Lundell, J.; Cohen, A.; Gerber, R. B. *J. Phys. Chem. A* **2002**, *106*, 11950.
(12) Khriachtchev, L.; Tanskanen, H.; Lundell, J.; Pettersson, M.; Kiljunen, H.; Rasanen, M. *J. Am. Chem. Soc.* **2003**, *125*, 4696.
(13) Feldman, V. I.; Sukhov, F. F.; Orlov, A. Y.; Tyulpina, I. V. *J. Am. Chem. Soc.* **2003**, *125*, 4698.
(14) Khriachtchev, L.; Tanskanen, H.; Cohen, A.; Gerber, R. B.; Lundell, J.; Pettersson, M.; Kiljunen, H.; Rasanen, M. *J. Am. Chem. Soc.* **2003**, *125*, 6876.
(15) Tanskanen, H.; Khriachtchev, L.; Lundell, J.; Kiljunen, H.; Rasanen, M. *J. Am. Chem. Soc.* **2003**, *125*, 16361.
(16) Baerends, E. J.; Autschbach, J.; Berger, J. A.; Bérces, A.; Bickelhaupt, F. M.; Bo, C.; Boeij, P. L. D.; Boerrigter, P. M.; Cavallo, L.; Chong, D. P.; Deng, L.; Dickson, R. M.; Ellis, D. E.; Faassen, M. v.; Fan, L.; Fischer, T. H.; Guerra, C. F.; Gisbergen, S. J. A. v.; Götz, A. W.; Groeneveld, J. A.; Gritsenko, O. V.; Grüning, M.; Harris, F. E.; Hoek, P. v. d.; Jacob, C. R.; Jacobsen, H.; Jensen, L.; Kadantsev, E. S.; Kessel, G. v.; Klooster, R.; Kootstra, F.; Krykunov, M. V.; Lenthe, E. v.; Louwen, J. N.; McCormack, D. A.; Michalak, A.; Neugebauer, J.; Nicu, V. P.; Osinga, V. P.; Patchkovskii, S.; Philipsen, P. H. T.; Post, D.; Pye, C. C.; Ravenek, W.; Rodriguez, J. I.; Romaniello, P.; Ros, P.; Schipper, P. R. T.; Schreckenbach, G.; Snijders, J. G.; Solà, M.; Swart, M.; Swerhone, D.; Velde, G. t.; Vernooijs, P.; Versluis, L. V., L.; Visser, O.; Wang, F.; Wesolowski, T. A.; Wezenbeek, E. M. v.; Wiesenekker, G.; Wolff, S. K.; Woo, T. K.; Yakovlev, A. L.; Ziegler, T. *ADF2008.01*; SCM, Theoretical Chemistry, Vrije Universiteit, Amsterdam, The Netherlands; Scientific Computing & Modelling NV, Amsterdam, The Netherlands, 2008.
(17) Bickelhaupt, F. M.; Baerends, E. J. In *Reviews in Computational Chemistry*; Lipkowitz, K. B., Boyd, D. B., Eds.; Wiley-VCH: New York, 2000; Vol. 15, p 1.
(18) Ziegler, T.; Rauk, A. *Theor. Chim. Acta* **1977**, *46*, 1.
(19) Ziegler, T.; Rauk, A. *Inorg. Chem.* **1979**, *18*, 1558.
(20) Ziegler, T.; Rauk, A. *Inorg. Chem.* **1979**, *18*, 1755.
(21) Kitaura, K.; Morokuma, K. *Int. J. Quantum Chem.* **1976**, *10*, 325.
(22) Becke, A. D. *Phys. Rev. A* **1988**, *38*, 3098.
(23) Perdew, J. P. *Phys. Rev. B* **1986**, *33*, 8822.
(24) te Velde, G.; Bickelhaupt, F. M.; Baerends, E. J.; Fonseca Guerra, C.; van Gisbergen, S. J. A.; Snijders, J. G.; Ziegler, T. *J. Comput. Chem.* **2001**, *22*, 931.
(25) Bickelhaupt, F. M.; van Eikema Hommes, N. J. R.; Fonseca Guerra, C.; Baerends, E. J. *Organometallics* **1996**, *15*, 2923.
(26) Hirshfeld, F. L. *Theor. Chim. Acta* **1977**, *44*, 129.
(27) Chang, C.; Pelissier, M.; Durand, P. *Phys. Scr.* **1986**, *34*, 394.
(28) Lindroth, E.; Heully, J. L.; Lindgren, I.; Martensson-Pendrill, A. M. *J. Phys. B* **1987**, *20*, 1679.
(29) van Lenthe, E.; Baerends, E. J.; Snijders, J. G. *J. Chem. Phys.* **1993**, *99*, 4597.
(30) van Lenthe, E.; Snijders, J. G.; Baerends, E. J. *J. Chem. Phys.* **1996**, *105*, 6505.
(31) van Lenthe, E.; van Leeuwen, R.; Baerends, E. J.; Snijders, J. G. *Int. J. Quantum Chem.* **1996**, *57*, 281.

(32) Morokuma, K. *Acc. Chem. Res.* **1977**, *10*, 294.
(33) Lignell, A.; Khriachtchev, L.; Lundell, J.; Tanskanen, H.; Rasanen, M. *J. Chem. Phys.* **2006**, 125.
(34) Panek, J. A.; Latajka, Z.; Lundell, J. *Phys. Chem. Chem. Phys.* **2002**, *4*, 2504.
(35) Pettersson, M.; Lundell, J.; Khriachtchev, L.; Rasanen, M. *J. Chem. Phys.* **1998**, *109*, 618.
(36) Tsivion, E.; Zilberg, S.; Gerber, R. B. *Chem. Phys. Lett.* **2008**, *460*, 23.
(37) Pimentel, G. C. *J. Chem. Phys.* **1951**, *19*, 446.
(38) Rundle, R. E. *J. Chem. Phys.* **1949**, *17*, 671.
(39) Last, I.; George, T. F. *J. Chem. Phys.* **1988**, *89*, 3071.
(40) Bickelhaupt, F. M.; Sola, M.; Fonseca Guerra, C. *J. Chem. Theory Comput.* **2006**, *2*, 965.
(41) Lein, M.; Frunzke, J.; Frenking, G. In *Optical Spectra and Chemical Bonding in Inorganic Compounds, Vol. 1*; Springer-Verlag Berlin: Berlin, 2004; Vol. 106, p 181.

JP903266A